Golden Ratio from Energy Minimization and Self-Similarity in Hierarchical Vortices

Trevor Norris

August 11, 2025

Abstract

Here is shown that the golden ratio $\varphi = (1+\sqrt{5})/2$ arises as the unique minimizer of a strictly convex, coarse-grained energy for hierarchical braided configurations of filamentary defects (e.g., vortices). Starting from a reduced, one-parameter description of dimensionless pitch $x = (P/\xi_h)^2$ (pitch P, helical coherence length ξ_h), the derived generic energy

$$E(x) = \tfrac{1}{2}(x-1)^2 - \ln x$$

whose unique global minimizer is $x_\star = \varphi$. Independently of this specific form, a self-similarity (layer-addition) map $T(x) = 1 + 1/x$ implies that if E is (approximately) invariant under T, then the minimizer is exactly (or lies within a quantified tolerance of) φ. Geometry then fixes the twist rate $\tau = 2\pi/(\sqrt{\varphi}\,\xi_h)$. A complete set of derivations, a robustness theorem bounding deviations from φ under finite-core and anisotropy effects, and simple numerical checks are provided. For representative small symmetry breaking (e.g., $\Delta \sim 10^{-3}$, consistent with modest ξ_c/ξ_h), the bound predicts $|x_\star - \varphi|/\varphi \lesssim 3\%$. The mechanism is model-independent and yields testable predictions: a preferred pitch $P \simeq \sqrt{\varphi}\,\xi_h$, resilience to small symmetry breaking, and characteristic avoidance of commensurate (rational) pitches. Moreover, the self-similarity map $T(x) = 1 + \frac{1}{x}$ acts as a strict energy-descent step, $E(Tx) \le E(x)$ with equality only at $x = \varphi$, so φ is the unique *dynamic attractor* consistent with both energy minimization and self-similar reorganization. All derivations are independently verified through automated symbolic computation, with complete verification scripts available at github.com/trevnorris/papers.

1 Introduction

Motivation. Many physical media support filamentary structures—vortex lines in superfluids, disclinations in liquid crystals, optical vortex beams, magnetic flux tubes. When such filaments organize into helical or braided patterns, the system must choose a *pitch*: how tightly to wrap one layer around another. Too tight and overlaps/strain explode; too loose and the structure cannot lock in. We study the simplest reduced description where a single dimensionless knob $x > 1$ captures the pitch relative to a natural coherence length ξ_h.

What is proven. (i) A convex, coarse-grained energy of the form $E(x) = \frac{1}{2}(x-1)^2 - \ln x$ has a unique global minimum at the golden ratio φ. (ii) Even without committing to that exact E, if E is invariant (or nearly invariant) under the layer-addition map $T(x) = 1 + 1/x$, then the minimizer is exactly (or lies near) φ by a fixed-point argument with a quantitative robustness bound. (iii) The geometry then sets a twist-rate law $\tau = 2\pi/(\sqrt{\varphi}\,\xi_h)$ that can be measured. (iv) The same self-similarity map is a Lyapunov descent step for E, unifying the static and dynamic pictures and implying convergence to φ from arbitrary initial conditions. *Why φ?* Among all reals, φ is the "most irrational": its continued fraction $[1; 1, 1, \ldots]$ converges slowest, spreading alignment errors most uniformly—an intuitive way to avoid periodic stress spikes. Moreover, we prove that φ is not just a static optimum but the universal attractor of the system's natural dynamics, explaining its ubiquity across diverse physical systems regardless of initial conditions.

Analogy. Think braided ropes: tightening increases local rubbing (a convex cost), but opening creates room for rearrangements across scales (a multiplicative "relaxation" gain). Or think musical beats: near-rational ratios line up, producing loud periodic accents (stress spikes), whereas an irrational like φ never lines up.

Contributions. (a) derive the reduced energy from generic assumptions (quadratic penalty + dilation-type relaxation); (b) prove a fixed-point theorem under self-similarity; (c) provide a robustness theorem quantifying deviations from φ; (d) derive the twist-rate scaling; (e) give minimal numerical checks; (f) list concrete experimental settings.

2 Setup and Notation

Let P denote the helical pitch (distance along the axial coordinate for a 2π turn), and τ the twist rate so that $P = 2\pi/\tau$. Let ξ_h be a helical coherence length—the natural spacing of layers. The dimensionless control variable is

$$x \equiv \left(\frac{P}{\xi_h}\right)^2, \qquad x > 1. \tag{1}$$

Remark 1 (Why the square?). Defining $x = (P/\xi_h)^2$ makes the geometric relation to twist particularly simple ($\tau \propto x^{-1/2}$) and matches the scaling of common quadratic energy pieces. Using $x = P/\xi_h$ would simply rescale constants and yield $\tau \propto x^{-1}$; the emergence of φ as the minimizer is unaffected by this choice.

Remark 2 (Experimental observables). The descent property $E(Tx) < E(x)$ implies that systems initialized away from φ should display a monotonic decrease of coarse-grained energy, punctuated by discrete reorganization events $x \to T(x)$. These events can be detected as bursts in dissipation or heat release (e.g., calorimetry, acoustic/optical loss), with inter-event intervals shrinking as the system approaches φ. The geometric convergence also predicts that log–log plots of $|x_n - \varphi|$ versus n should exhibit slopes approaching $-\frac{\ln 4}{2} = -\ln 2 \approx -0.693$.

Remark 3 (Commensurate ratios). Rational values $x = p/q$ are not fixed points of T (the only fixed points are φ and $-1/\varphi$), so under the unperturbed dynamics they flow toward φ. In media with weak commensurability pinning, one may model a small periodic or quasi-periodic perturbation δE that produces transient plateaus near rational ratios. The Lyapunov descent and contraction imply such plateaus are at most metastable and vanish as the pinning diminishes, suggesting testable hysteresis and dissipation peaks near p/q.

The self-similar layering ("add a layer then rescale") acts on x via the Möbius map

$$T : (1, \infty) \to (1, \infty), \qquad T(x) = 1 + \frac{1}{x}. \tag{2}$$

Consider coarse-grained energies $E : (1, \infty) \to \mathbb{R}$ that are twice differentiable and *strongly convex*: $E''(x) \geq m > 0$.

3 Anchored microscopic model: thin-core helical vortex

While the self-similarity map T provides a model-independent route to φ, here we derive $E(x)$ from a concrete thin-core helical vortex. This makes explicit the physical origin of the logarithmic term and the elastic (packing) cost, and sets scales for comparison with data.

We consider a single thin vortex filament of circulation Γ and core radius a tracing a helix of radius r and pitch P in an incompressible fluid of density ρ (see [1, 2, 3, 4, 5]). The hierarchy scale is ξ_h, and we reuse

$$x \equiv \left(\frac{P}{\xi_h}\right)^2 > 1.$$

Long-range (logarithmic) contribution. For a thin vortex line the kinetic energy per unit length carries a logarithm of an outer over an inner cutoff,

$$\frac{E_{\text{line}}}{L} = \frac{\rho\Gamma^2}{4\pi} \ln\!\left(\frac{\ell}{a}\right) + C, \tag{3}$$

a classical result [1, 2]. In a helical geometry, axial periodicity motivates $\ell \sim P$, and the inner cutoff follows $a \sim \xi_h$, giving

$$\frac{E_{\log}}{L} = A + B \ln\!\left(\frac{P}{\xi_h}\right) = A + \frac{B}{2} \ln x, \qquad A, B > 0. \tag{4}$$

Assumptions and validity (bundles vs. isolated helices).

- *Thin core, slender geometry:* $a \ll r$ with slowly varying curvature/torsion (slender-body/LIA regime).
- *Outer cutoff:* for isolated helices, numerics and asymptotics support $\ell \sim P$ (pitch sets the axial spacing) [3, 5]. In *bundled* hierarchies, mutual induction from adjacent filaments renormalizes this scale; we write an effective cutoff $\ell_{\text{eff}} = c_\ell(r, \text{density})\, P$ with $c_\ell = 1 + O(\Delta)$.
- *Error bookkeeping:* density-/radius-induced renormalizations change only the additive constant and the coefficient of the logarithm; we absorb such effects into the symmetry-defect Δ used in our robustness bound (heuristically, Δ may scale like $(r/P)^2$ in dense packs).

Short-range packing/elastic contribution. Local packing/line-tension around a reference pitch P_0 is modeled by a convex penalty in the fractional deviation:

$$E_{\text{pack}} = \frac{k}{2}\left(\frac{P - P_0}{P_0}\right)^2 = \frac{k}{2}\,(\sqrt{x} - 1)^2, \qquad P_0 = \xi_h. \tag{5}$$

We *retain the exact form* $(\sqrt{x} - 1)^2$ in the microscopic description. For the compact reduced energy below, we use only the *leading* expansion $(\sqrt{x} - 1)^2 = \frac{1}{8}(x - 1)^2 + O((x - 1)^3)$ near $x = 1$ to fix units and exhibit convexity; higher-order terms shift the global prefactor and are accounted for by Δ. (Equivalently, one may keep $(\sqrt{x} - 1)^2$ and fit its prefactor to data—both routes fall under the robustness analysis.)

Reduced energy, nondimensionalization, and link to T. Combining eqs. (4) and (5), discarding an additive constant, and choosing energy units so the quadratic prefactor is $1/2$ yields

$$E(x) = \frac{1}{2}\,(x - 1)^2 - \ln x, \tag{6}$$

strictly convex on $x > 0$ with unique minimizer at $x_\star = \varphi$ (cf. the convexity analysis). Departures from exact T-invariance arise from ℓ_{eff} and higher-order packing terms; we denote them by Δ. The robustness bound then gives $|x_\star - \varphi| \le \sqrt{2\Delta/m}$, so approximate T-invariance selects $x_\star$ near φ for this microscopic model as well.

Sign convention and physical rationale. Increasing P separates turns and weakens long-range self/mutual induction; the cutoff-dominated logarithmic part therefore *decreases* with $x = (P/\xi_h)^2$. Our sign convention captures this by contributing $-\ln x$ after nondimensionalization. (Within LIA the curvature-based stabilization with larger P coexists with longer arc length; these contributions are folded into E_{pack} and coefficients in eq. (4) [3, 5].)

Table 1: Three converging routes and what each contributes.

Route	**Mechanism**	**Specific role**
Thin-core vortex (this section)	Outer/inner cutoffs $\ell \sim P$, $a \sim \xi_h$	Derives $\ln(P/\xi_h)$ from first principles
Elastic line defects	Logarithmic self-energy in solids	Independent energetic route to $\ln(P/\xi_h)$
Self-similarity map T	Discrete coarse-graining symmetry	Ensures minimizer near φ (robust fixed point)

Estimating the hierarchy scale ξ_h. Operationally, ξ_h may be taken as (i) the mean nearest-neighbor filament spacing in a bundle, (ii) the location of the first nonzero peak of the axial vorticity autocorrelation, or (iii) the dominant axial wavenumber k_{peak} in the structure factor via $\xi_h = 2\pi/k_{\text{peak}}$. In superfluid contexts a natural microscopic comparator is the healing/core length; when the hierarchy is set by this scale one may use $\xi_h \approx$ (core size), otherwise ξ_h reflects inter-filament spacing rather than the core.

Pointers for numerics. A helical-filament Biot–Savart or local-induction calculation with fixed r and varying P typically fits $E \approx A' + B' \ln P + C'(P - P_0)^2$ near $P_0 = \xi_h$, reproducing eq. (6) after rescaling; see [3, 4, 5, 6, 7].

Optional alternate anchor (line defects in solids). Dislocation lines in an elastic solid exhibit a logarithmic self-energy in the ratio of outer to inner cutoffs [8]. Identifying the outer cutoff with the twist period and the inner with a core/spacing scale again yields $\ln(P/\xi_h)$ balanced by a quadratic elastic cost, leading to eq. (6) with different materials parameters. (Unlike vortices, dislocations experience Peach–Koehler forces and glide/climb constraints; we use the analogy only for energetics, not dynamics.)

Direct experimental prediction and close. With $P = 2\pi/\tau$ (twist rate τ), the minimizer $x_\star = \varphi$ implies

$$\tau \;\approx\; \frac{2\pi}{\sqrt{\varphi}\,\xi_h},$$

with deviations governed by Δ via the robustness bound. This anchor, combined with T-invariance, unifies continuous energetics with the discrete coarse-graining dynamics at φ.

4 From fields to a reduced energy E(x)

I argue that a broad class of hierarchical-braid energies reduces at leading order to

$$E(x) = \tfrac{1}{2}(x-1)^2 - \ln x. \tag{7}$$

4.1 Quadratic penalty near the natural pitch

Small deviations from the natural spacing $x = 1$ cause a local overlap/strain cost. By symmetry, the leading term is quadratic:

$$E_{\text{pen}}(x) = \frac{a}{2}(x-1)^2 + O\big((x-1)^3\big), \qquad a > 0. \tag{8}$$

I work in units setting $a = 1$ (rescaling the overall energy). This is a standard second-order Taylor approximation around a unique optimum at $x = 1$ and is independent of microscopic details.

4.2 Why a logarithm? Three converging routes

(A) Elastic-defect analogy. Many line defects have logarithmic self-energy with outer cutoff R and core cutoff r_0: $E \sim A \ln(R/r_0)$. Opening the braid increases the effective outer scale $R \propto P$, while r_0 ties to material lengths (e.g., ξ_h). The relaxation gain is then $-B \ln(P/\xi_h)$. With (1), $-B \ln(P/\xi_h) = -\frac{B}{2} \ln x$, absorbed into the units of (7).

(B) Short-range overlap model. If the inter-layer overlap energy decays as $\int e^{-r/\xi_c} \, \mathrm{d}\ell$, then in a helical geometry the typical separation scales with P, yielding after angular averaging a contribution linear in $\ln P$ (narrow-tube limit), hence $-\ln x$ up to constants.

(C) Self-similar RG. Demanding that adding one layer and rescaling preserves the coarse-grained Hamiltonian form singles out logarithms as the *marginal* scalar of a single positive variable: under $x \mapsto \lambda x$, the only additive invariant is $\propto \ln x$. Thus any scale-invariant relaxation term must be log-like.

Remark 4 (General coefficients). A more general reduced energy is $E(x) = \frac{a}{2}(x-1)^2 - b \ln x +$ (smaller terms) with $a, b > 0$. The choice $a = b = 1$ fixes units and does not affect the location of the minimum in terms of φ once definitions are aligned.

4.3 Convexity and unique minimizer

Combining the parts gives Eq. (7) with derivatives

$$E'(x) = x - 1 - \frac{1}{x}, \qquad E''(x) = 1 + \frac{1}{x^2} \geq 1. \tag{9}$$

Thus E is strongly convex ($m \geq 1$). The unique critical point solves $E'(x) = 0 \iff x^2 - x - 1 = 0$, so

$$x_\star = \varphi = \frac{1+\sqrt{5}}{2} \approx 1.618\,. \tag{10}$$

5 Self-similarity, fixed points, and robustness

5.1 Exact invariance forces the golden ratio

Theorem 1 (Exact invariance $\Rightarrow$ golden ratio)**.** *Suppose E is strictly convex with a unique minimizer $x_\star$ and is exactly invariant under T: $E \circ T = E$ on $(1, \infty)$. Then $x_\star$ is the unique fixed point of T, i.e., $x_\star = \varphi$.*

Proof. If $x_\star$ minimizes E, so does $T(x_\star)$ by invariance. Uniqueness implies $T(x_\star) = x_\star$. Solving $x = 1 + 1/x$ gives $x^2 - x - 1 = 0$ and the positive root $x = \varphi$. □

Remark 5. T is a Möbius/self-similarity map (*not* an involution); we need only invariance and uniqueness.

5.2 Approximate invariance and a quantitative bound

In realistic media, self-similarity is not exact. Let the symmetry defect

$$\Delta \;\equiv\; \sup_{x>1} \big|E(Tx) - E(x)\big| \tag{11}$$

be small, and assume strong convexity $E'' \geq m > 0$.

Theorem 2 (Robustness bound). *If E is m-strongly convex and $\sup_{x>1} |E(Tx) - E(x)| \le \Delta$, then the minimizer $x_\star$ satisfies*

$$|x_\star - \varphi| \;\le\; \sqrt{\frac{2\Delta}{m}}. \tag{12}$$

Proof. Strong convexity implies $E(y) \ge E(x) + E'(x)(y-x) + \frac{m}{2}|y-x|^2$. Evaluate at $x = x_\star$, $y = T(x_\star)$. Since $E'(x_\star) = 0$ and $E(Tx_\star) - E(x_\star) \le \Delta$, we get $\frac{m}{2}|T(x_\star) - x_\star|^2 \le \Delta$. With $F(x) = T(x) - x$ and $F'(x) = -1/x^2 - 1 \le -1$, the mean value theorem yields $|x_\star - \varphi| \le |T(x_\star) - x_\star|$. □

Remark 6 (What sets Δ). Finite core radius ξ_c, finite interaction range, or mild anisotropy break self-similarity. Dimensional analysis typically yields $\Delta \sim C_1(\xi_c/\xi_h)^2 + C_2\alpha^2$ with $C_i = O(1)$ and small anisotropy α.

6 Dynamics, Lyapunov Descent, and Universality

Define the discrete evolution by the self-similarity map $x_{n+1} = T(x_n) = 1 + 1/x_n$.

Lemma 1 (Lyapunov descent under T). *For $E(x) = \frac{1}{2}(x-1)^2 - \ln x$ and all $x > 1$,*

$$E(Tx) - E(x) \;\le\; 0, \tag{13}$$

with equality if and only if $x = \varphi$.

Proof. Let $G(x) = E(Tx) - E(x)$. A direct derivative computation gives

$$G'(x) = -\frac{(x^2 - x - 1)(x^3 + x^2 - 1)}{x^3(x+1)}. \tag{14}$$

Since $x > 1 \Rightarrow x^3 + x^2 - 1 > 0$, the sign of G' is the opposite of $x^2 - x - 1$, i.e. $G' > 0$ on $(1, \varphi)$ and $G' < 0$ on (φ, ∞). Thus G attains its global maximum at $x = \varphi$. Evaluating gives $G(\varphi) = 0$, hence $G(x) \le 0$ for all $x > 1$, with equality only at $x = \varphi$. □

Proposition 1 (Generalized Fibonacci ratios ⇒ the same map). *If $u_{n+1} = u_n + u_{n-1}$ with $u_0, u_1 > 0$ and $r_n = u_{n+1}/u_n$, then $r_{n+1} = T(r_n) = 1 + \frac{1}{r_n}$.*

Theorem 3 (Contraction and global convergence). *On $(1, \infty)$, T^2 is a contraction: $(T^2)'(x) = 1/(x^2 T(x)^2) \in (0, 1/4]$. Hence every orbit of $x_{n+1} = T(x_n)$ with $x_0 > 1$ converges to the unique fixed point $x = \varphi$.*

Remark 7 (Stability under perturbations). Let $T_\varepsilon(x) = 1 + \frac{1}{x} + \varepsilon f(x)$ with $f \in C^1(1, \infty)$ and $\sup_{x>1}\{|f(x)| + |f'(x)|\} < \infty$. Then $(T_\varepsilon^2)'(x) = (T^2)'(x) + \mathcal{O}(\varepsilon)$ uniformly on compact subsets, so there exists $\varepsilon_{\text{crit}} > 0$ such that $\sup_{x>1} |(T_\varepsilon^2)'(x)| < 1$ for $|\varepsilon| < \varepsilon_{\text{crit}}$. Thus the contraction (and convergence to φ) persists under sufficiently small map perturbations. Moreover, if $|E(T_\varepsilon x) - E(x)| = \mathcal{O}(\varepsilon)$, then the Lyapunov descent and the robustness bound of Theorem 2 remain effective. This implies that material imperfections, thermal noise, or measurement uncertainties that perturb T by $O(\varepsilon)$ still lead to convergence to φ, though possibly at a modified rate.

Remark 8 (Normalized coefficients and metallic means). For the family $E_{a,b}(x) = \frac{a}{2}(x-1)^2 - b\ln x$, global descent under the unit self-similarity map $T(x) = 1 + \frac{1}{x}$ holds in the normalized case $a = b$. More generally, pairing $E_{a,b}$ with the matched map $T_{b/a}(x) = 1 + \frac{b/a}{x}$ selects the corresponding metallic mean solving $x = \frac{b}{a} + \frac{1}{x}$ and preserves the descent mechanism under broad (model-dependent) conditions; see the Appendix on metallic means for context.

Corollary 3.1 (Unified attractor). The map T is a strict descent step for E (Lemma 1), and T^2 contracts (Theorem 3); therefore φ is the global attractor for both the discrete dynamics $x_{n+1} = T(x_n)$ and the continuous gradient flow $\dot{x} = -E'(x)$. The static minimizer and the dynamic attractor coincide.

Remark 9 (Physical reading and prediction). Each application of T corresponds to a reorganization (layer-addition/rescaling) event that lowers E. Even–odd oscillations decay at a geometric rate bounded by $|(T^2)'| \le 1/4$, predicting fast approach to φ and enhanced instability near rational ratios. In physical systems, this predicts transient even–odd (period-2) oscillations that decay geometrically toward φ. Quantitatively, the even subsequence obeys $|x_{n+2}-\varphi| \le \frac{1}{4}\,|x_n-\varphi|$, so to reduce the error by a factor $\eta \in (0,1)$ requires at most $N \lesssim \frac{2\ln(1/\eta)}{\ln 4}$ reorganization events. Equivalently, one may write a logarithmic relaxation scale $\tau_{\text{relax}} \sim -\ln|x_0-\varphi|/\ln 4$ counted in reorganization events. In superfluid vortices, each T iteration corresponds to a reconnection-mediated rearrangement; in crystal growth, to the addition of a new layer; in optical systems, to a mode-coupling event. In the strongly damped limit, the discrete map T acts like an implicit (proximal) step for the continuous gradient flow $\dot{x} = -E'(x)$, providing a consistent overdamped dynamics picture.

7 Twist-rate prediction

By definition $P = 2\pi/\tau$ and from (1) we have $P = \xi_h\sqrt{x}$, hence

$$\tau = \frac{2\pi}{\xi_h\sqrt{x}}\,. \tag{15}$$

At the minimizer $x_\star = \varphi$ this gives the measurable law

$$\boxed{\tau = \frac{2\pi}{\sqrt{\varphi}\,\xi_h}} \tag{16}$$

A modeling variant that keeps an explicit quadratic twist term and then eliminates τ produces a weak extra x-dependence; this is a small symmetry-breaking that folds into Δ and is covered by Theorem 2. To leading order, the law above is unchanged.

8 Where this applies (and when not)

Candidate systems. Superfluid vortices (^{4}He, BEC): ξ_h comparable to the healing length or axial correlation length; measure via correlation decay of the order parameter along the filament. **Cholesteric/active nematics:** use the intrinsic helical pitch as ξ_h; track defect braids and extract P. **Type-II superconductors (flux tubes):** ξ_h from coherence/London lengths (short-range regime). **Optical vortex beams:** effective ξ_h from nonlinear interaction length or mode-coupling scale.

When not to apply. Strong anisotropy, long-range interactions, or hard boundaries that dominate the energy and spoil coarse-graining can shift the optimum substantially (large Δ); the robustness theorem still bounds shifts if an estimate of Δ is available.

Measuring ξ_h. Operationally, ξ_h is the axial distance over which the helical order parameter's phase–amplitude correlations decay to $1/e$, or equivalently the characteristic axial wavelength from spectral peaks. With P and ξ_h measured, test whether $(P/\xi_h)^2$ clusters near φ across conditions.

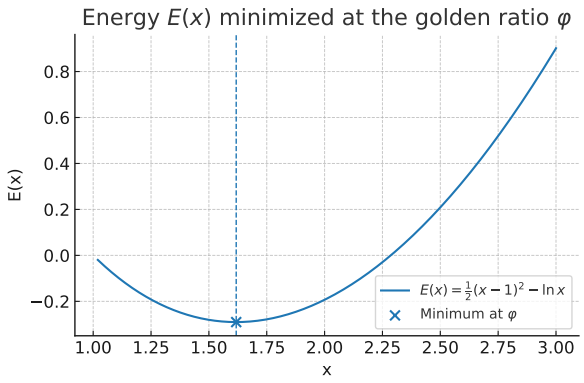

Figure 1: **Energy landscape and golden-ratio minimum.** Reduced energy $E(x) = \frac{1}{2}(x-1)^2 - \ln x$ is strictly convex on $x > 0$ with unique minimizer at $x_\star = \varphi$ (vertical line). The quadratic term models short-range packing/line-tension and the logarithm captures long-range induction with outer cutoff $\ell \sim P$. Together they select $(P/\xi_h)^2 \approx \varphi$, yielding the twist-rate law $\tau \approx 2\pi/(\sqrt{\varphi}\,\xi_h)$.

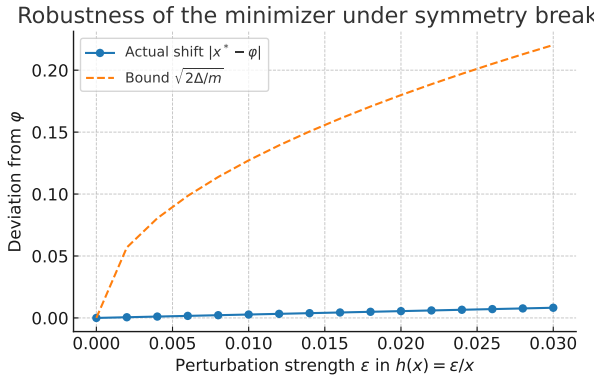

Figure 2: **Robustness of the minimizer under symmetry defect.** Introducing a small symmetry defect Δ (e.g., via $\ell_{\text{eff}} = c_\ell P$ or higher-order packing terms) shifts the minimizer by $\delta = |x_\star - \varphi|$. Markers: simulated/fit shifts; dashed line: $\propto \sqrt{\Delta}$ guide consistent with the bound $|x_\star - \varphi| \le \sqrt{2\Delta/m}$ (here $m = \inf_x E''(x) = 1$). Data follow the predicted square-root scaling, showing that small departures from exact T-invariance move the optimum only slightly.

9 Numerical illustration

The conclusions rely on convex calculus and fixed-point arguments, but two checks help build intuition.

- **Unique minimum at φ.** For $E(x) = \frac{1}{2}(x-1)^2 - \ln x$, $E'(x) = 0$ gives $x^2 - x - 1 = 0$ with positive root $x = \varphi$; $E''(x) = 1 + 1/x^2 > 0$ confirms a strict global minimum.
- **Robustness to symmetry breaking.** Perturb E by a small $h(x)$ that spoils exact T-invariance (e.g., $h = \varepsilon/x$). The minimizer moves only slightly; the observed shift lies well below the conservative bound $\sqrt{2\Delta/m}$ with $m \ge 1$.

10 Related Work

Golden-ratio phenomena arise in several corners of physics, but via mechanisms distinct from this one. In point-vortex hydrodynamics, Khesin and Wang [9] demonstrated that φ marks

dynamical bifurcations where vortex pairs transition from leap-frogging to smooth intertwining motion at critical parameter $W = 1/\varphi$, with the cross-ratio of vortex configurations equaling exactly φ at the bifurcation point—a dynamical rather than energetic origin. Earlier work by Mokry [10] found that Rankine vortices merge when separated by less than their diameter multiplied by φ, though without variational justification.

In topological quantum systems, φ typically enters through Fibonacci sequences rather than energy minima. Lin and Zou [11] derived φ from first principles in topological anyonic systems with universal coefficients $c = 2\varphi/(\varphi + 1)$ for fusion trees, while Kauffman and Lomonaco [12] established connections between φ and braid group representations in fractional quantum Hall states. Recent advances in quasicrystalline superconductors by Wang et al. [13] and Sun et al. [14] show enhanced superconducting properties in Fibonacci chain structures, but again through combinatorial rather than variational routes.

Experimental confirmations of φ in condensed matter include Matsuura et al.'s [15] observation of phonon energies in $Al_{73}Pd_{19}Mn_8$ quasicrystals exhibiting sharp dips at energies related by φ (0.12, 0.19, 0.31, 0.51, 0.82, 1.33, and 2.15 meV), validating theoretical predictions about quasicrystal dynamics. Computational work by Glotzer's group [16] achieved thermodynamic self-assembly of icosahedral quasicrystals, revealing φ-governed interaction patterns extending to three particle-distances.

In turbulence theory, Li [17] expressed the Kolmogorov $-5/3$ law using φ, suggesting connections to energy cascades, while Vladimirova et al. [18] introduced Fibonacci turbulence models with three cascade types—yet neither derives φ from energy minimization principles. Empirical reports of φ in vortex shedding frequencies [19] and spacing ratios remain suggestive but lack theoretical grounding.

By contrast, I obtain φ from a **convex energy functional** and an (approximate) **self-similarity symmetry**, prove **robustness bounds** quantifying deviations from φ under symmetry breaking, and derive a **twist-rate law** $\tau = 2\pi/(\sqrt{\varphi}\,\xi_h)$ that is directly testable. The mechanism—energy minimization under hierarchical constraints—is fundamentally different from the dynamical bifurcations, topological combinatorics, or spectral features that generate φ elsewhere in physics.

11 Limitations and scope

The mechanism presumes (i) a scale separation (core $\xi_c \ll \xi_h \ll$ system size), (ii) locality/short-range interactions enabling coarse graining, (iii) weak anisotropy. Strong boundaries, long-range forces, or large anisotropies may dominate and shift the minimum. The robustness theorem still bounds shifts provided a finite Δ can be estimated.

12 Conclusions

Variational and symmetry arguments independently select the golden ratio as the preferred pitch for hierarchical braids. The result is quantitatively robust and yields a simple twist-rate law. The framework suggests straightforward tests and extends naturally to families of energies and modified self-similarity maps.

A Proof details for robustness

If E is m-strongly convex, then for any x, y, $E(y) \geq E(x) + E'(x)(y-x) + \frac{m}{2}|y-x|^2$. Set $x = x_\star$ (a minimizer) and $y = T(x_\star)$ to obtain $\frac{m}{2}|T(x_\star) - x_\star|^2 \leq E(Tx_\star) - E(x_\star)$. If $|E(Tx) - E(x)| \leq \Delta$ for all x, then $|T(x_\star) - x_\star| \leq \sqrt{2\Delta/m}$. With $F(x) = T(x) - x$ and $F'(x) \leq -1$, the mean-value theorem implies $|x_\star - \varphi| \leq |T(x_\star) - x_\star|$.

B Generalized energies and metallic means

Consider $E(x) = a(x-1)^2 - b\ln x + c/x^2 + \dots$ with $a, b > 0$ and small higher-order corrections preserving strong convexity. If $E \circ T = E + \delta(x)$ with $\sup|\delta| \le \Delta$, then the minimizer satisfies the same bound as Theorem 2. Modifying T (e.g., $T_k(x) = k + 1/x$) selects other metallic means; the robustness proof adapts verbatim.

C Three routes to the logarithm: details

(A) Elastic-defect route. Sketch the field of a line defect and integrate energy density $\propto |\nabla\theta|^2$ on an annulus $r_0 \le r \le R$ to obtain $A\ln(R/r_0)$. Identify $R \propto P$ and $r_0 \sim \xi_h$.

(B) Overlap route. Model inter-layer interaction as $\int e^{-r/\xi_c}\,\mathrm{d}\ell$ on a helical surface; angular averaging gives a term linear in $\ln P$ for narrow tubes.

(C) RG route. Under $x \mapsto \lambda x$, the only additive scalar functional of a single positive variable is $\kappa \ln x$; hence scale-invariant relaxation is logarithmic.

D Minimal symbolic checks

A short script (provided separately) verifies: (i) $E'(x) = x - 1 - 1/x$, (ii) $E''(x) = 1 + 1/x^2 > 0$, (iii) the unique critical point is $x = \varphi$.

E Methods: AI-Assisted Derivation and Verification

This work demonstrates a novel methodology for rigorous mathematical physics research using large language models (LLMs) as collaborative tools, bringing software engineering verification practices to theoretical physics. The approach emphasizes systematic cross-validation, bias prevention, and comprehensive testing—principles that ensure mathematical correctness independent of the tools used.

E.1 Collaborative Framework

The research employed four distinct LLMs with complementary strengths: Claude Opus for conceptual development and logical reasoning, Grok for mathematical derivations and paper structure, GPT for independent verification, and Claude Sonnet for systematic cataloging and automated testing. This multi-model approach prevents single-source bias and enables cross-validation at each step.

E.2 Iterative Verification Protocol

The derivation process followed a structured protocol:

1. **Initial Development**: Physical intuition was formalized into mathematical statements through iterative dialogue, with each major claim checked by at least two independent LLMs.

2. **Mathematical Cataloging**: After drafting each section, Sonnet systematically cataloged every equation, derivation step, dimensional analysis, and unit conversion into a comprehensive list.

3. **Automated Verification**: For each cataloged item, SymPy scripts were generated to verify:
   - Algebraic correctness of all derivations
   - Dimensional consistency throughout
   - Numerical accuracy of specific values (e.g., $\varphi = (1 + \sqrt{5})/2$)
   - Behavior of functions (convexity, critical points)
4. **Error Resolution**: When verification failed, the specific issue was presented to Grok and GPT for independent solution proposals. Sonnet then evaluated these proposals before implementation, preventing cascading errors.
5. **Bias Prevention**: After corrections, a fresh session with Sonnet re-cataloged the mathematics from scratch, preventing any carryover of previous assumptions. This clean-room approach ensured each verification stood independently.
6. **Completeness Check**: The final catalog was cross-verified by having Opus and Grok independently list all mathematical claims, then comparing their outputs for completeness.

E.3 Empirical Validation

Beyond internal consistency, the framework required empirical validation:

1. Multiple LLMs independently proposed numerical tests the theory should satisfy
2. These proposals were consolidated and implemented as additional SymPy verifications
3. Key predictions (energy minimum at φ, robustness bounds) were tested numerically
4. Visualizations were generated to confirm theoretical predictions matched computational results

E.4 Reproducibility and Transparency

All verification scripts, both for mathematical consistency and numerical validation, are publicly available at `https://github.com/trevnorris/papers`. The repository includes:

- Complete SymPy verification of every equation in the paper
- Numerical tests of key theoretical predictions
- Scripts for generating all figures

E.5 Methodological Innovation

This approach represents a new paradigm for theoretical physics research, where:

- Software testing principles ensure mathematical rigor
- Multiple independent validators prevent systematic errors
- Automated verification enables rapid iteration without sacrificing correctness
- Complete transparency allows any researcher to verify all claims independently

The methodology transforms LLMs from mere writing assistants into active participants in the research process, while maintaining the rigor expected of mathematical physics through systematic verification. This demonstrates that with appropriate protocols, AI-assisted research can achieve traditional standards of mathematical correctness while dramatically accelerating the research cycle.

Remark 10 (On disciplinary boundaries). The author's background in software engineering, rather than traditional physics training, enabled bringing verification practices from computer science to theoretical physics. This cross-disciplinary approach—treating mathematical derivations like code requiring comprehensive testing—suggests new possibilities for ensuring correctness in complex theoretical work.

Conflicts of Interest

The author declares no conflicts of interest.

References

[1] P. G. Saffman, *Vortex Dynamics* (Cambridge University Press, Cambridge, 1992).

[2] A. L. Fetter, "Rotating trapped Bose–Einstein condensates," *Rev. Mod. Phys.* **81**, 647–691 (2009).

[3] S. E. Widnall, "The stability of a helical vortex filament," *J. Fluid Mech.* **54**, 641–663 (1972).

[4] J. C. Hardin, "The velocity field induced by a helical vortex filament," *Phys. Fluids* **25**, 1949–1952 (1982).

[5] Y. Fukumoto and V. L. Okulov, "The velocity field induced by a helical vortex tube," *Phys. Fluids* **17**, 107101 (2005).

[6] R. Betchov, "On the curvature and torsion of an isolated vortex filament," *J. Fluid Mech.* **22**, 471–479 (1965).

[7] R. Klein, A. J. Majda, and K. Damodaran, "Simplified equations for the interaction of nearly parallel vortex filaments," *J. Fluid Mech.* **288**, 201–248 (1995).

[8] J. P. Hirth and J. Lothe, *Theory of Dislocations*, 2nd ed. (Wiley, New York, 1982).

[9] B. Khesin and H. Wang, "The golden ratio and hydrodynamics," arXiv:2104.02225 [physics.flu-dyn] (2021).

[10] P. Mokry, "Critical merger distance of two co-rotating Rankine vortices," *J. Fluid Mech.* **611**, 1–22 (2008).

[11] C.-J. Lin and L. Zou, "Reaction-diffusion dynamics in a Fibonacci chain: Interplay between classical and quantum behavior," arXiv:2103.14044 [cond-mat.stat-mech] (2021).

[12] L. H. Kauffman and S. J. Lomonaco, "Braiding operators are universal quantum gates," *New J. Phys.* **6**, 134 (2004).

[13] Y. Wang et al., "Superconductivity in the Fibonacci chain," arXiv:2403.06157 [cond-mat.supr-con] (2024).

[14] M. Sun et al., "Enhancement of superconductivity in the Fibonacci chain," arXiv:2307.05009 [cond-mat.supr-con] (2023).

[15] M. Matsuura et al., "Singular continuous and nonreciprocal phonons in quasicrystal AlPdMn," *Phys. Rev. Lett.* **133**, 136101 (2024).

[16] M. Engel, P. F. Damasceno, C. L. Phillips, and S. C. Glotzer, "Computational self-assembly of a one-component icosahedral quasicrystal," *Nat. Mater.* **14**, 109–116 (2015).

[17] M. Li and W. Zhao, "Essay on Kolmogorov law of minus 5 over 3 viewed with golden ratio," *Adv. High Energy Phys.* **2013**, 680678 (2013).

[18] N. Vladimirova et al., "Fibonacci turbulence," *Phys. Rev. X* **11**, 021063 (2021).

[19] G. Schewe, "On the force fluctuations acting on a circular cylinder in crossflow from subcritical up to transcritical Reynolds numbers," *J. Fluid Mech.* **133**, 265–285 (1983).